ACS OMEGA

http://pubs.acs.org/journal/acsodf

Article

Characterization of Pore Structures with Mercury Intrusion Porosimetry after Electrochemical Modification: A Case Study of Jincheng Anthracite

Junqing Guo,* Xiaoyu Zhang, Chunsheng Lu, Zhaoyun Chai, Guanxian Kang, Guofei Zhao, Tianhe Kang, Shirui Zhang, and Hengzhong Li

Cite This: *ACS Omega* 2022, 7, 11148−11157

Read Online

ACCESS | Metrics & More | Article Recommendations

ABSTRACT: Quantitative characterization of the change in the cleat and pore structures and fractal dimensions in anthracite after electrochemical modification is crucial for better understanding of the modification effect. Thus, lump anthracite samples were electrochemically modified in our manufactured device with 0, 0.5, 1, and 2 V/cm potential gradients. The changes in heterogeneity and porosity after modification were tested and analyzed by mercury intrusion porosimetry (MIP) and fractal theory. The results indicated that the total volume of the pores increased after electrochemical treatment and continuously increased with increasing potential gradient during the treatment process. After modification, the number of pores or fractures with a pore size between 6 and 20 μm in coal after modification increases significantly. According to the intrusion pressure, three stages were defined as lower (P_M < 0.1 MPa), intermediate (0.1 ≤ P_M < 10 MPa), and higher regions (P_M ≥ 10 MPa), which are characterized by fractal dimensions D_1, D_2, and compression stages, respectively. After modification, the fractal dimension D_1 showed an increasing trend, while the fractal dimension D_2 showed a decreasing trend, indicating that the fracture system became more complicated and that the pore system became more regular after electrochemical treatment. The evolution mechanism of heterogeneity and porosity and their fractal dimensions were explained by the dissolution of minerals, change in pH values, and dynamics of temperatures during the process of modification. The results obtained in this work are of important guiding significance for coalbed methane (CBM) extraction via in situ modification by electrochemical treatment.

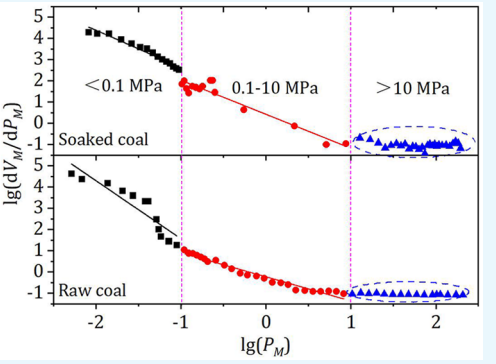

1. INTRODUCTION

In recent years, unconventional resources such as coalbed methane (CBM), shale gas, and tight sandstone gas have attracted widespread attention, and the exploitation theory and technology are developing rapidly.[1] However, commercial gas production has been hampered by the low permeability of coal seams in China.[2,3] Thus, permeability-improving methods, including protective seam mining,[4] hydraulic fracturing,[5,6] hydraulic cutting,[7,8] microwave modification,[9] and blasting-induced fracturing,[10,11] increase massive fractures in coal seams, which greatly reduce gas pressure in the early stage of extraction and improve the gas extraction rate. However, extraction is difficult in the later stage because of little variation in gas pressure and a lack of driving force,[12] and the generated coal fines block fractures and boreholes and further cause permanent damage to permeability.[13] In addition, the lump coals cut by cracks are still large, and some studies indicate that even an inch of lump coal requires months or years to release most of its gas.[14,15] Eddy et al. reported that the residual gas content can be as high as 38%.[16]

To accelerate CBM extraction, Kang reported an exploratory study on intensifying methane desorption and seepage from coal modified by electrochemical treatment.[17] Zhang et al. found that the amount of adsorbed CH_4 on coal samples decreased after electrochemical modification due to the change in functional groups on the coal surface.[18] Guo et al. found that the average desorption rate of methane from 130 to 140 mm lump coal after electrochemical treatment increased by 1.68 times, reaching desorption equilibration.[19] The desorption ratio and diffusion coefficient of CH_4 on Jincheng anthracite increased after electrochemical modification in ion electrolytes.[20] In addition, Kang and Zhang et al. both found that the pores and fractures increased after electrochemical treatment

Received: December 26, 2021
Accepted: March 8, 2022
Published: March 25, 2022

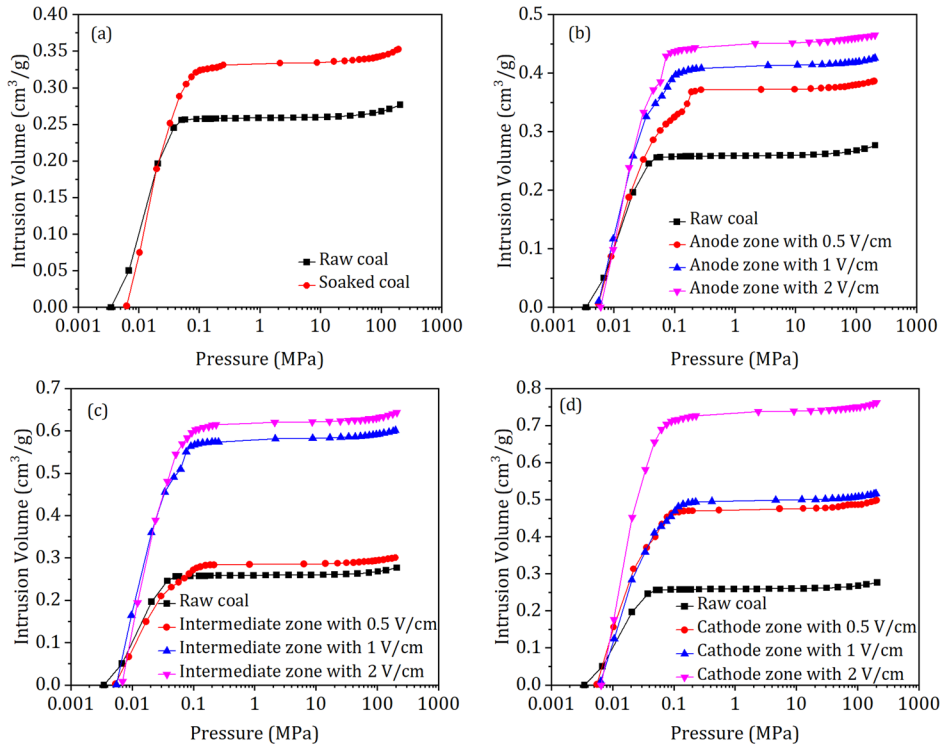

Figure 1. Mercury intrusion curves of lump anthracite samples before and after electrochemical treatment: (a) raw and soaked sample, (b) modified samples at the anode zone, (c) modified samples at the intermediate zone, and (d) modified samples at the cathode zone.

of electrolytic dissolution of minerals and electrophoresis migration of charged particles such as coal powder and clay, which provides a gas migration pathway.[21,22] Additionally, the adsorbed gas can be stripped from the coal surface and driven by electro-osmosis and heat, which provides an impetus for gas migration. Mercury intrusion porosimetry (MIP), low-pressure nitrogen gas adsorption (LP-N_2GA), and CO_2 adsorption have been used to characterize the macropores, mesopores, and micropores in the coal matrix, as well as the secondary porosity composed of cleats.[22−25] The total porosity of coal varies with the coal rank[26,27] and can be up to 20%, exceptionally as high as 50% due to the development of microfractures in high-rank coal.[28,29] Li et al. observed the nanoscale pore structures of coals by combined atomic force microscope (AFM) and SEM technologies and reported that it is effective in revealing pore structures and mechanical properties.[30] Li et al. reported that, for CO_2 displacing CH_4, more CO_2 can be adsorbed on the nanoscale pore surface of coal, resulting in higher CH_4 desorption.[31] The pore structures change after electrochemical modification (mentioned above) discussed mainly the evolution of surface area, pore volume, and pore size, but the quantitative characterization of the change of pore fractal dimensions still needs better understanding.

The fractal dimension (D), a dimensionless index, is used to quantify the complexity of the pore/fracture distribution.[32] Combining LP-N_2GA test data and MIP test results, Steele and Angulo et al. reported the Frenkel−Halsey−Hill (FHH) model and fractal dimension of pore structures in coals.[33,34] Sarkar and Chaudhuri proposed that the heterogeneity of pore distribution can also be obtained by digital images by scanning electron microscopy (SEM) and CT.[35] The change in fractal characteristics of pores in coals after cyclical modification has been achieved by Su et al. with nuclear magnetic resonance techniques and LP-N_2GA, and the results showed that the fractal dimensions of the adsorption pores decreased after modification.[36]

However, research on the effects of electrochemical modification on the pore structures and fractal dimensions of lump anthracite is limited. In this work, we electrochemically modified lump anthracite samples with 0, 0.5, 1, and 2 V/cm electric potential gradients. The pore structures and fractal dimensions of lump anthracite samples before and after modification were tested by MIP and SEM techniques. The pores were reclassified into four zones according to their degree of complexity, which was reasonable to characterize the pore structures of electrochemically modified lump anthracite. On the basis of fractal theory, the changes in heterogeneity and porosity were further analyzed.

2. RESULTS AND DISCUSSION

2.1. Mercury Intrusion Curves. Figure 1 shows the mercury intrusion curves of lump anthracite samples before and after electrochemical treatment. The maximum mercury intrusion of raw coal samples was 0.28 cm^3/g, increasing to 0.35 cm^3/g after immersion in a Na_2SO_4 electrolyte for 120 h (Figure 1a), and further increasing to 0.39, 0.43, and 0.47 cm^3/g after modification with 0.5, 1, and 2 V/cm electric potential gradients in the anode zone (Figure 1b), increasing by 39.3%, 53.6%, and 67.9%, respectively. Figure 1c and d also show that the maximum mercury intrusion increases after electrochemical modification and further increases with increasing electric potential gradients. In addition, the modification effect at the cathode zone is most obvious, followed by the intermediate zone and the anode zone. The MIP test results indicate that the total volume of the pores increased after electrochemical treatment and continuously increased with increasing potential gradient during the treatment process.

https://doi.org/10.1021/acsomega.1c07286
ACS Omega 2022, 7, 11148−11157

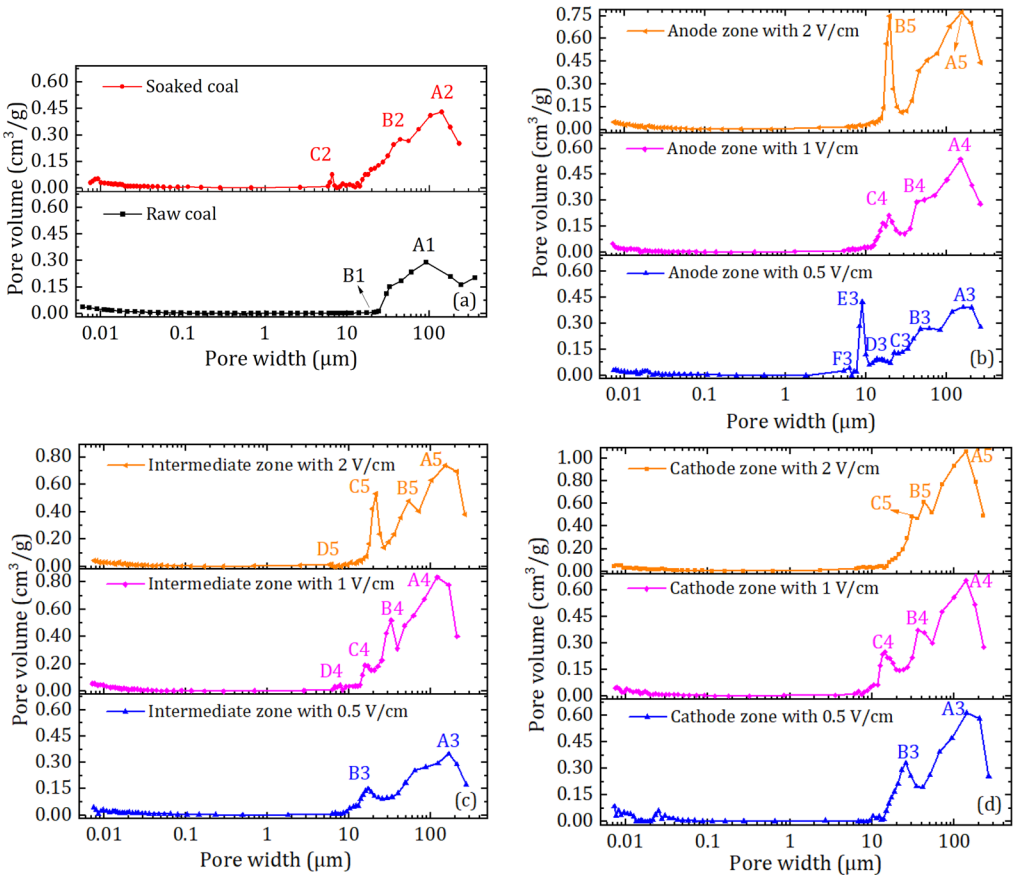

Figure 2. Pore size distribution of coal samples modified with 0 V/cm (a) and 0.5, 1, and 2 V/cm at the anode zone (b), intermediate zone (c), and cathode zone (d).

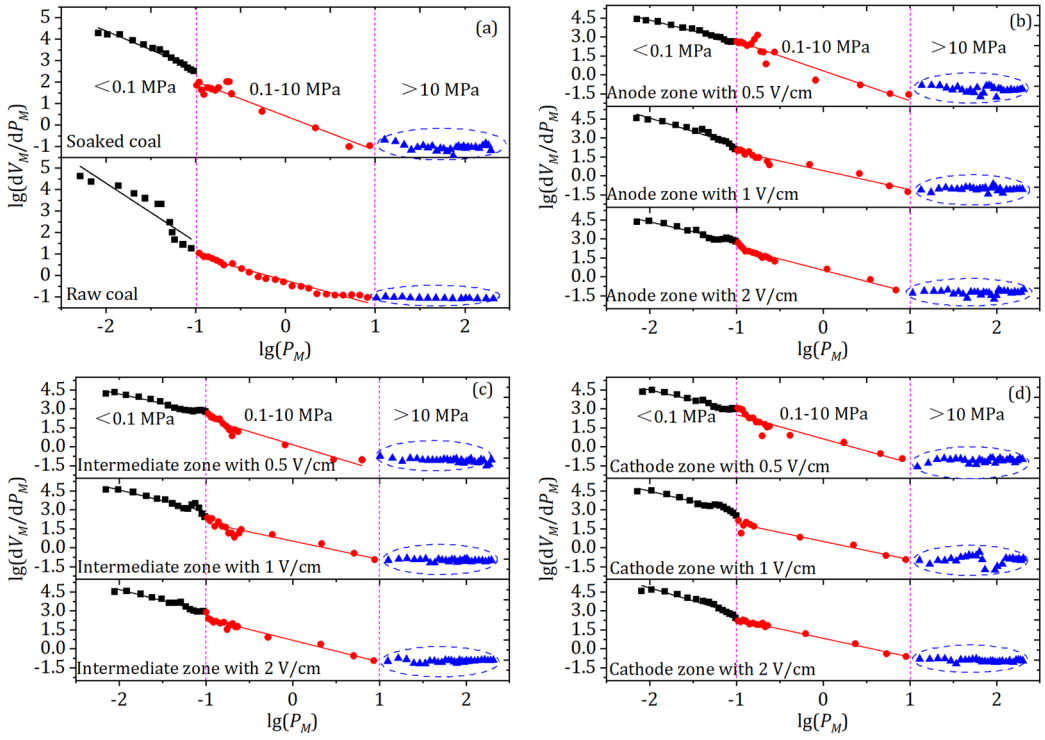

Figure 3. Relationship between $\log(dV_M/dP_M)$ and $\log(P_M)$ based on anthracite sample MIP data after electrochemical modification with 0 V/cm (a) and 0.5, 1, and 2 V/cm at the anode zone (b), intermediate zone (c), and cathode zone (d).

https://doi.org/10.1021/acsomega.1c07286
ACS Omega 2022, 7, 11148−11157

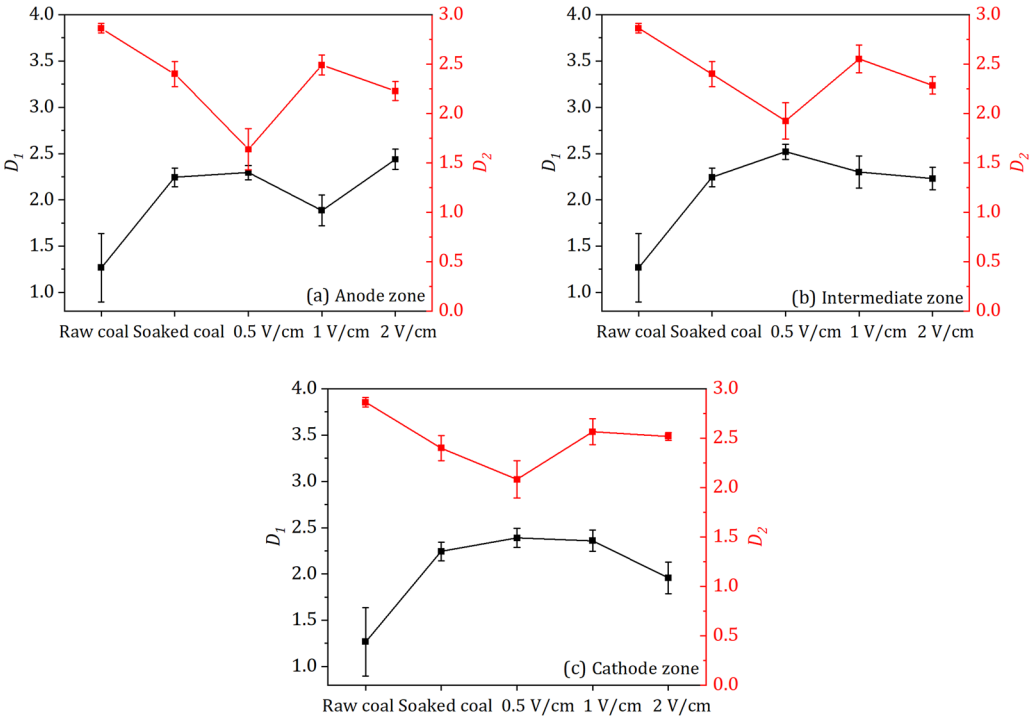

Figure 4. Change of fractal dimension after electrochemical modification at different anthracite zones: (a) anode zone, (b) intermediate zone, and (c) cathode zone.

2.2. Change of Pore Size Distribution. Figure 2 shows the pore size distributions of raw anthracite, soaked anthracite, and modified anthracite with different electric potential gradients in the anode zone, intermediate zone, and cathode zone. As seen from Figure 2a, with decreasing pore width, the pore volume of raw anthracite increases sharply and reaches a peak value at a pore size of approximately 91.2 μm (A1), while the pore volume decreases sharply and reaches a low value at a pore size of approximately 20 μm (B1), and the pore volume increases slightly when the pore size is greater than 0.1 μm. After soaking in Na_2SO_4 solution for 120 h and drying at 378−383 K, there are two new peak values at pore sizes of approximately 44.6 and 6.6 μm (C2 and B2, respectively), indicating that the number of pores and fractures in soaked coal increases. The same results were also found by Xia et al.,[37] who observed new holes on the anthracite coal surface via SEM images. Figure 2b, c, and d show the pore size distributions of coal samples modified in the anodic, intermediate, and cathodic zones, respectively. After electrochemical modification, the number and value of pore volume peaks increased. The values of the A1 peak of raw anthracite coal increased from 0.289 cm^3/g to 0.35−1.06 cm^3/g, and the pore width increased from approximately 91.2 μm to 120−165 μm, which indicated that the number of fractures obviously increased.[19] After modification, the new peaks at pore sizes ranging from 6 to 50 μm indicate that the number of pores or fractures with a pore size between 6 and 20 μm in coal after modification increases significantly.[38]

2.3. Change of Fractal Dimension. The Menger sponge model is suitable for calculating the fractal dimension D of pores based on mercury injection tests.[39−41] According to the Washburn equation, the radius r of pores filled with mercury at pressure P_M is expressed as[42]

$$P_M = \frac{2\sigma \cos\theta}{r} \tag{1}$$

where σ is the surface tension of mercury (0.48 N/m) and θ is the mercury−coal contact angle (130°). The relationship between the pore size distribution dV_M/dr and the fractal dimension D is[43]

$$\frac{dV_M}{dr} \propto r^{2-D} \tag{2}$$

Combining eqs 1 and 2, we get:

$$\frac{dV_M}{dP_M} \propto P_M^{D-4} \tag{3}$$

That is

$$\log\left(\frac{dV_M}{dP_M}\right) \propto (D-4)\log P_M \tag{4}$$

where V_M is the volume of cumulative mercury injection, which is approximated by pore volume in cm^3/g; P_M is the pressure of mercury injection, MPa; and r is the radius of pores, μm. Figure 3 shows the fractal region curves of lump anthracite samples using the Menger sponge model. All of the curves were divided into three regions: lower (P_M < 0.1 MPa) and intermediate (0.1 ≤ P_M < 10 MPa), which are characterized by D_1 and D_2, respectively. Although the higher regions (P_M ≥ 10 MPa) had strong piecewise fractal characteristics, the fractal dimensions of the pores underwent a drastic change to values higher than 3. A similar conclusion was also found by Toda and Toyoda, and Zwietering and Krevelen reported that the phenomenon can be attributed to the compressibility of the coal samples.[44,45]

The change in anthracite fractal dimensions (D_1 and D_2) after electrochemical modification with different electric

https://doi.org/10.1021/acsomega.1c07286
ACS Omega 2022, 7, 11148−11157

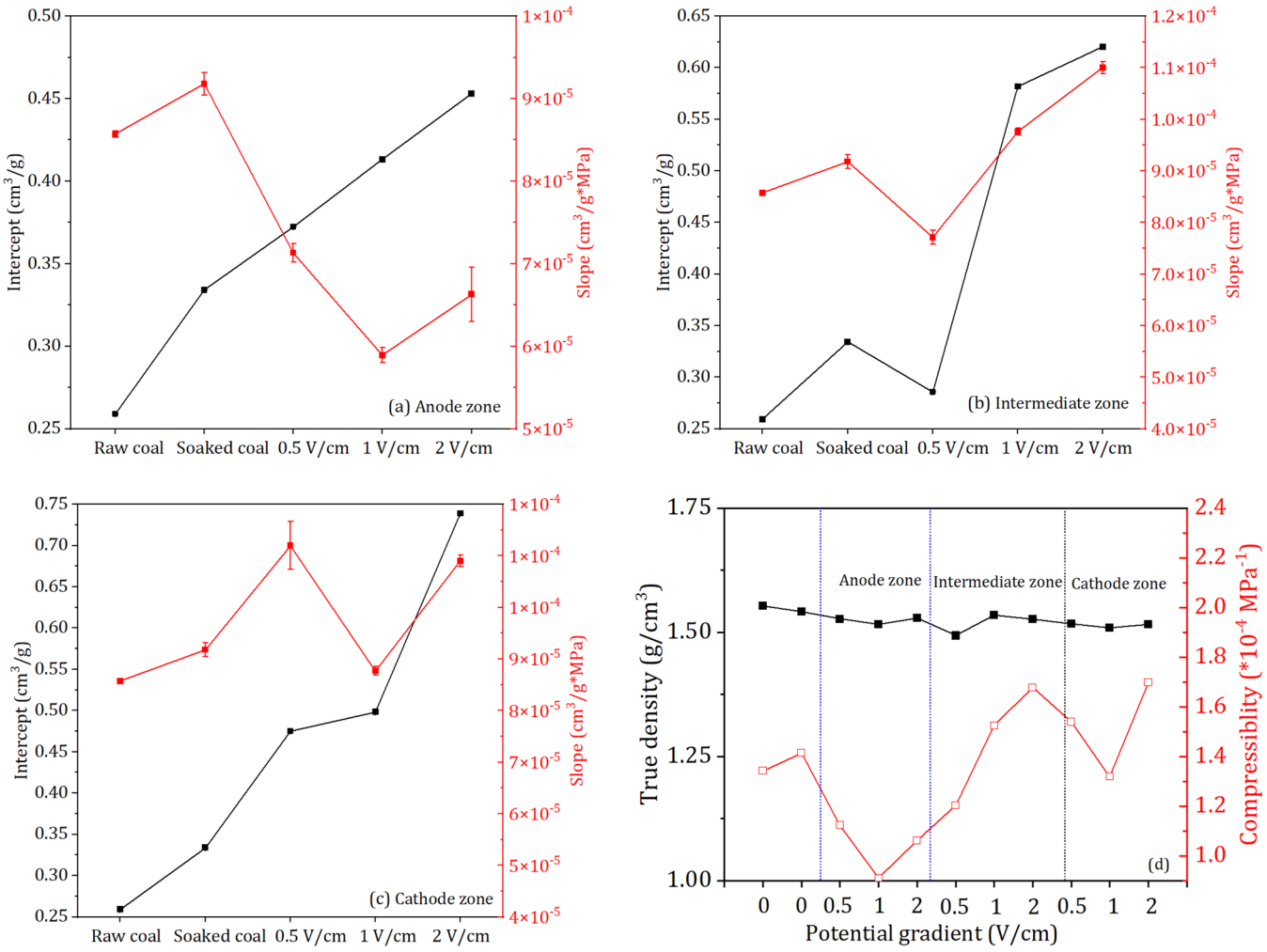

Figure 5. Linear fitting results of intercept and slope at the anode zone (a), intermediate zone (b), and the cathode zone (c) and true density and compressibility (d).

potential gradients at the anode zone, intermediate zone, and cathode zone is shown in Figure 4. As shown in Figure 4, the fractal dimension D_1 was comparatively low and showed an increasing trend after electrochemical modification, while the fractal dimension D_2 showed a decreasing trend. The comparatively low fractal dimension of D_1 indicates that the fractures in anthracite are developed in an orderly manner. Similar results were also illustrated in previous work that anthracite coal has a mutually orthogonal and fully developed structure of fractures, which was observed by optical microscopy.[46] The fractal dimension D_2 is 2.86, which is consistent with the calculation result of Zhao et al.[47] that the range of fractal dimensions is 2.27−2.97, and the pore structure of tested anthracite coal is relatively complicated. After modification, the fractal dimensions D_1 approximately showed an increasing trend with increasing electric potential gradients, while the fractal dimensions D_2 showed a decreasing trend, which indicates that the fracture system became more complicated and the pore system became more regular after electrochemical treatment because the filled minerals in fractures are dissolved and macropores are formed.

In the higher-pressure regions ($P_M \geq 10$ MPa), there is a rectilinear relationship between high pressure and the volume of mercury intrusion. The intercept at the ordinate of the linear fitting results represents the pore volume that excludes compressibility, and the change in intercept after modification is shown in Figure 5. The volume of injected mercury at pressure 0.2 MPa is the cleat volume, and the pore volume of the coal matrix can be calculated by eq 15. The compressibility of the original and soaked samples was 1.342×10^{-4} and 1.414×10^{-4} MPa^{-1}, respectively. After modification, the compressibility changes to $(0.91-1.698) \times 10^{-4}$ MPa^{-1}. In general, the compressibility of the sample modified in the anodic zone decreases, while the compressibility of the sample modified in the intermediate and cathodic zones increases because the electrophoresis treatment is more obvious in the intermediate and cathodic zones, which migrates the coal particles and clay and makes the coal matrix disperse. Guo et al.[46] also found a positive relationship between the porosity and coal matrix compressibility. Combined with the analysis in section 3 and the fact that the incremental instruction is very low when the pore size is larger than 6 μm, the increase in pore volume is due primarily to mercury intrusion into the cleats >25 μm wide, cleats ranging in width from 6 to 25 μm, and coal matrix pores ranging in aperture from 100 nm to 6 μm at lower, low, and intermediate pressures, respectively. Gamson et al.[48] also found that the cleats in coal are commonly 5−20-μm-wide and infilled by minerals using SEM.

2.4. Effect of Electrochemical Treatment on the Porosity of Anthracite Coal. Table 1 shows the pore

https://doi.org/10.1021/acsomega.1c07286
ACS Omega 2022, 7, 11148−11157

Table 1. Pore Structure Parameters of Coal Samples before and after Modification

coal samples	cleat volume (m/g)	average cleat width (μm)	cleat porosity (%)	pore volume (m/g)	average pore width (nm)	porosity (%)
raw coal	0.1290	27.51	15.20	0.0012	114	0.12
soaked coal	0.1649	38.73	19.24	0.0043	308	0.42
S_{3a}	0.1835	68.09	26.15	0.005	437	0.56
S_{4a}	0.2035	61.79	29.87	0.0061	530	0.69
S_{5a}	0.2234	61.21	30.57	0.0062	398	0.65
S_{3i}	0.1396	51.97	20.92	0.0059	827	0.73
S_{4i}	0.2867	60.35	33.24	0.0087	497	0.76
S_{5i}	0.2901	58.51	36.92	0.0096	592	0.87
S_{3c}	0.2332	60.51	28.22	0.0086	731	0.81
S_{4c}	0.2447	63.18	34.02	0.0087	564	0.90
S_{5c}	0.3217	69.86	37.01	0.0153	765	1.20

structure parameters of the raw coal and modified coal samples. The cleat volume, average cleat width, and cleat porosity of the original sample are 0.129 mL/g, 27.51 μm, and 15.2%, respectively, similar to the research results of other scholars.[27,28] In addition, the average diameter of pores ranging from 100 nm to 6 μm is 114 nm, and the coal matrix porosity is 0.12%, indicating that endogenous fractures (cleats) in anthracite occupy a considerable proportion of the total porosity. After soaking in Na_2SO_4 solution and drying, the average cleat width of coal increase to 38.73 μm, which increases the cleat porosity to 19.24%, and the average pore size of the coal matrix increases to 308 nm, which increases the matrix porosity to 0.42%. After modification, the average cleat diameter, cleat porosity, coal matrix porosity, and average pore size of the modified samples increase to 51.97−69.86 μm, 398−827 nm, 20.92−37.01%, and 0.56−1.2%, respectively, indicating that the cleat porosity and coal matrix porosity of the sample obviously increase by electrochemical modification and are positively related to the potential gradient.

2.5. Modification Mechanism Discussion of Anthracite Pore Structure. Figure 6 shows the SEM images of the dissolution and disappearance of minerals filled in the fractures of coal in the anodic and immediate zones before and after electrochemical treatment and the appearance of fractures of coal in the cathodic zone. Figure 6a shows that two fractures with widths of 10−30 μm cross each other at an approximately 80° angle, and the cleat is filled with minerals, such as carbonate and sulfide. After treatment, the minerals disappear (shown in Figure 6b). The carbonate in the cleats is dissolved by hydrogen ions produced in the anodic zone during electrochemical processes because of the oxidation reaction.[50] The reaction equation is as follows:

$$CaCO_3 + 2H^+ \rightarrow Ca^{2+} + CO_2 + H_2O \quad (5)$$

Figure 6c and d show SEM images of the disappearance of minerals filled in cleats and pores of coal in the immediate zone before and after treatment. Figure 6c shows that there is a mineral-filled cleat with a width of 1−20 μm, and some minerals are embedded in the coal matrix. Gamson et al.[45] measured the microstructures in coals using SEM and observed that there are five types of microfractures recognized between the larger cleats: vertical cleats, horizontal cleats, blocky fractures, conchoidal fractures, and striae. These microfractures are often mineralized. After treatment, the microfractures and pores were unblocked (see Figure 6d) due to the electrolysis dissolution and electrophoresis migration of minerals.[18] The emergence of these microfractures can build pathways for gas migration from pores to fractures. Figure 6e and f show SEM images of the appearance of fractures of coal in the cathodic zone. Figure 6e shows that the coal matrix surface is tight and flat. After treatment, mesh fractures with widths of 5−50 μm appeared on the coal surface (see Figure 6f), which may be due to the removal of coal or clay particles in the coal matrix in the action of electrophoresis or washing out by the electrolyte in the action of electroosmosis.

3. CONCLUSIONS

To accelerate the CBM exploration process, the application of electrochemical modification makes the pore system of the lump anthracite more regular and the fracture system more

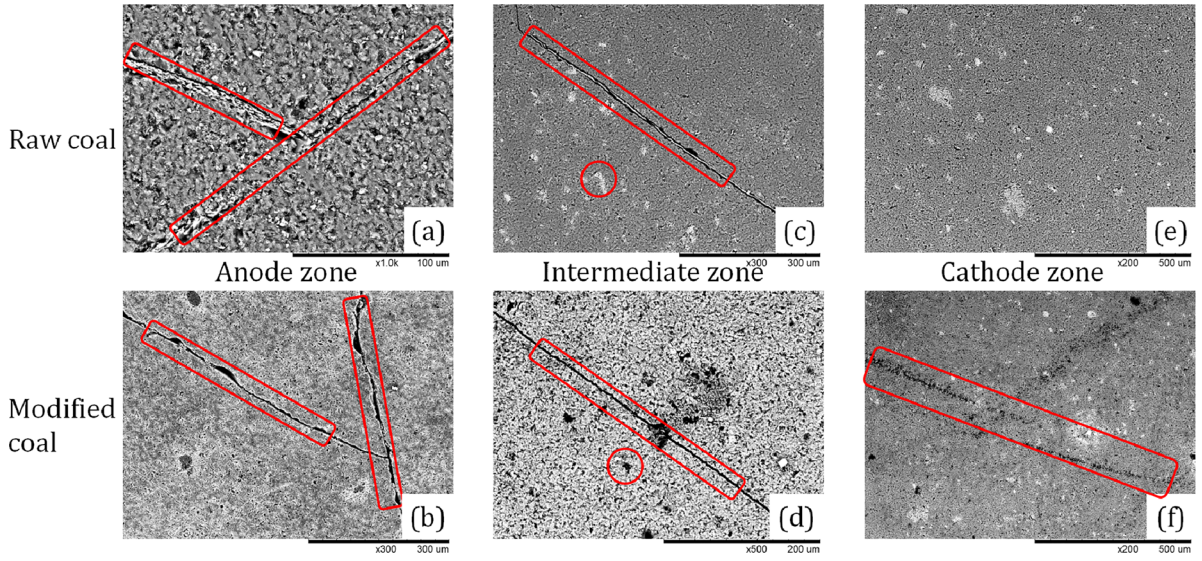

Figure 6. SEM images of the dissolution and disappearance of minerals filled in cleats of coal in the anode zone (a and b) and intermediate zone (c and d) and the appearance of fractures of coal in the cathode zone (e and f).

https://doi.org/10.1021/acsomega.1c07286
ACS Omega 2022, 7, 11148−11157

Table 2. Coal Properties

		analysis wt %			ultimate analysis %				maceral composition %		
coal sample	vitrinite reflectance %	moisture	ash yield	volatile matter	C	H	O	S	vitrinite	inertinite	liptinite
anthracite	2.86	1.65	5.21	6.12	86.52	2.64	6.83	3.32	86.3	13.7	0.0

Table 3. Composition of the Ash Yield

	ash composition %								
coal sample	SiO_2	Al_2O_3	CaO	Fe_2O_3	SO_3	MgO	TiO_2	Na_2O	P_2O_5
anthracite	24.83	22.14	11.87	26.27	10.81	0.9	0.09	0.19	0.13

complex, and the modification effect becomes more obvious with increasing potential gradient.

After modification, the porosity and the cleats with widths of 9 and 20 μm obviously increase due to the dissolution of carbonate in the cleats, and the coal/clay particles in the coal matrix in the cathodic zone are washed out by electrophoresis and electroosmosis.

The effect of modification with different potential gradients on Qinshui Basin anthracite coal is discussed above, which is not enough for the guiding of CBM extraction. More of the effect of electrochemical modification parameters like electrode materials and electrolyte types on coal pore and fracture structures and more test means for the characterization of pore and fracture structures like CO_2/N_2 adsorption and small X-ray scattering will be analyzed in future research.

4. EXPERIMENTAL SECTION

4.1. Coal Sample. The anthracite used was collected from the No. 15 coal seam in the southeastern Qinshui Basin from the Sihe Coal Mine (Shanxi Province, China). Table 2 and Table 3 summarize the sample details, including petrologic and chemical analyses. Sampling has to be based on vitrinite band. Some cubes with side lengths of approximately 1 cm were processed from the samples to document microstructures in at least three principal planes: the face cleat, the butt cleat, and the bedding. The sample cubes had a total mass of 2.5 kg and were divided randomly into five groups for electrochemical modification at different potential gradients.

4.2. Experimental Apparatus. The electrochemical modification equipment shown schematically in Figure 7 is composed of a direct current (DC) power source, current meter, wire, electrolyzer, electrolyte, electrodes, and coal samples. The output voltage of the DC power source is 0–250 V. The electrolyte is a solution of Na_2SO_4. The electrode is a square graphite sheet with a thickness of 5 mm and side lengths of 100 mm.

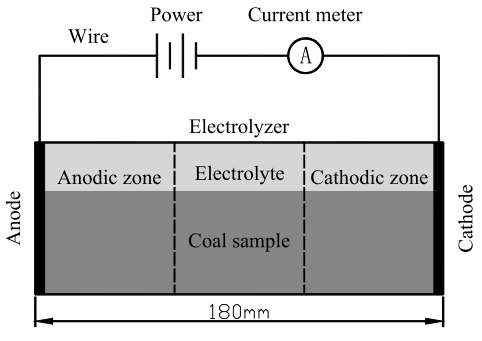

Figure 7. Diagram of electrochemical modification equipment.

4.3. Experimental Schemes. To investigate the change in the pore-fracture structure of the samples under different electrochemical treatments, 11 experimental schemes were designed, as shown in Table 4. Scheme S_1 was used to investigate the pore-fracture structure of the original sample. Scheme S_2 was used to investigate the pore-fracture structure with electrolyte soaking and power off, and schemes S_{3a}–S_{5c} were used to investigate the pore-fracture structure after modification under different electric gradients from 0.5 to 2 V/cm.

Table 4. Experimental Schemes

scheme	coal sample	potential gradient (V/cm)	time (h)	He denisity (g/cm^3)
S_1	raw coal			1.5501
S_2	soaked coal	0	120	1.5415
S_{3a}	modified coal at anode zone	0.5	120	1.5269
S_{4a}	modified coal at anode zone	1	120	1.5161
S_{5a}	modified coal at anode zone	2	120	1.5283
S_{3i}	modified coal at intermediate zone	0.5	120	1.4933
S_{4i}	modified coal at intermediate zone	1	120	1.5344
S_{5i}	modified coal at intermediate zone	2	120	1.5265
S_{3c}	modified coal at cathode zone	0.5	120	1.5175
S_{4c}	modified coal at cathode zone	1	120	1.5095
S_{5c}	modified coal at cathode zone	2	120	1.5160

4.4. Experimental Process. The samples were modified with the experimental apparatus, according to the experimental schemes shown in Table 4. In the process of modification, the pH values and temperature of the electrolyte in the anodic, intermediate, and cathodic zones were measured using a pH meter and thermometer, respectively. After 120 h, the samples were labeled S_{na}, S_{ni}, and S_{nc} sequentially according to anodic, intermediate, and cathodic zones, where n is 3, 4, and 5. In addition, the original sample and modified sample were labeled S_1 and S_2, respectively. Then, the samples were cleaned with distilled water and dried in an oven at 378–383 K until a constant weight was achieved. True densities of the samples were measured by helium displacement using a Quantachrome UltraPyc 1000 helium pycnometer, and the helium density results are shown in Table 4.

4.5. Experimental Phenomenon. In the process of modification, an oxidizing reaction occurs at the anode where

https://doi.org/10.1021/acsomega.1c07286
ACS Omega 2022, 7, 11148–11157

oxygen is formed, and a reduction reaction occurs at the cathode where hydrogen is formed. The reaction equations are as follows:

$$2H_2O - 2e^- \rightarrow O_2 + 4H^+ \text{ (at the anode)} \quad (6)$$

$$2H_2O + 2e^- \rightarrow H_2 + 2OH^- \text{ (at the cathode)} \quad (7)$$

Because of the electrolytic reaction, the electrolyte pH in the anodic zone decreases while the pH in the cathodic zone increases. The H^+ ions travel to the cathode, and the OH^- ions travel to the anode under the action of an electric field. The electrolyte pH in the intermediate zone is between the pH in the anodic and cathodic zones. The electrolyte pH values in the three zones in schemes 3−11 after modification are shown in Figure 8 and were 2.1−3.2, 6−8.3, and 8.3−11.2.

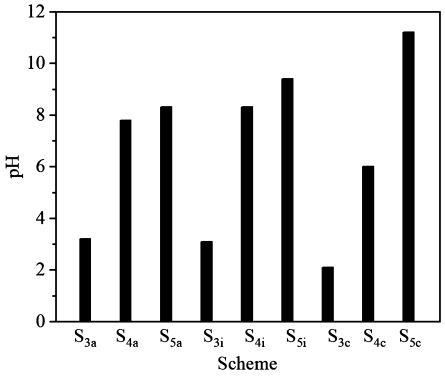

Figure 8. pH of three zones of electrolyte in different schemes after modification.

Figure 9 shows the brown precipitate produced in the process of modification of coal samples in the cathodic zone.

Figure 9. Brown precipitate produced in the process of coal modification.

The appearance of this precipitate is due primarily to Fe^{3+} generated by electrochemical dissolution of pyrite in anthracite in the anodic zone traveling to the cathode and generating $Fe(OH)_3$ in combination with OH^-. The reaction equations are as follows:

$$FeS_2 + 8H_2O \rightarrow Fe^{3+} + 2SO_4^{2-} + 16H^+ + 15e^- \quad (8)$$

$$Fe^{3+} + 3OH^- \rightarrow Fe(OH)_3 \quad (9)$$

Figure 10 shows the temperature histogram of the electrolyte when the modification has just finished. The

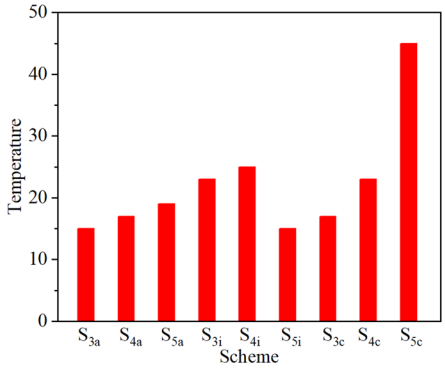

Figure 10. Temperature of electrolyte in different schemes after modification.

temperature increases from 13.4 °C to 17.3−35.1 °C and increases with increasing potential gradient.

To gain insight into the change in pore structure of coal samples after modification, fractal analysis of the samples was performed. Pfeifer and Avnir[51] stated that the injection curve of pore structure with a fractal characteristic obeys the following relationship:

$$\log\left(\frac{dV_p}{dr}\right) \propto (2 - D_s)\log(r) \quad (10)$$

where V_p is the cumulative injection volume at a given pore radius r and D_s is the surface fractal dimension. The relational equation will be obtained between the cumulative injection volume V_p derivative with respect to pressure p and the surface fractal dimension D_s.

$$\log\left(-\frac{dV_p}{dp}\right) \propto (4 - D_s)\log(p) \quad (11)$$

Using this equation, the fractal dimension can be calculated.

5. PORE-FRACTURE STRUCTURE OF COAL BY MIP AND SEM

5.1. MIP. MIP is based on the gradual injection of mercury into an evacuated pore system with external pressures. When the pressure is greater than 20 MPa, coal can be compressed, and compressibility affects the test results. Friesen and Mikula[52] found that the porosity of coal particles can be corrected based on fractal theory. For the coal particles, the pressure regime is trisected by three different fractal dimensions. In order of increasing pressure, the injection volume corresponds to interparticle penetration, pore penetration, and compressibility.

Because the test sample is a piece of coal and microfractures are developed, the injected mercury volume at low pressure can represent the fracture volume. Laubach et al.[53] found that endogenous fractures (cleats) are developed in a more orderly manner than fractures in adjacent noncoal rocks and that the cumulative frequency (f) of cleats having apertures of e or larger follows a power law:

$$f = be^{-c} \quad (12)$$

where b is a general measure of the cleat intensity and c is a constant (referred to as the fractal dimension). The formula indicates that the cleat system of coal has self-similarity. Therefore, the fractal dimension of cleats in coal can be

https://doi.org/10.1021/acsomega.1c07286
ACS Omega 2022, 7, 11148−11157

calculated using MIP results. In combination with the research results of other scholars on the fractal dimension of coal particles, for the lump coal, at least three fractal dimensions such as D_1 and D_2 can be obtained. In order of increasing pressure, these fractal dimensions correspond, respectively, to cleat penetration, pore penetration, and coal matrix compressibility. If the values of D_1 and D_2 are distinctively different, the cleat and pore can be distinguished according to the intersection of their corresponding curves, and cleat structure parameters such as cleat volume, average cleat width, and cleat porosity can be further calculated. The cleat volume is the volume of injected mercury corresponding to the curve intersection. The average cleat width d_f can be calculated as follows:

$$d_f = 4V_f/S_f \tag{13}$$

where V_f is the cleat volume, mL/g, and S_f is the surface area of the cleat, $m^2 \cdot g^{-1}$. The cleat porosity is calculated as follows:

$$\phi_f = V_f/(V_f + V_m + V_{mp}) \tag{14}$$

where V_m is the coal matrix skeleton volume, which can be calculated by coal mass and helium density,[49] and V_{mp} is the coal matrix pore volume, which can be calculated as follows:

$$V_{mp} = V_t - V_f - V_{co} \tag{15}$$

where V_t is the total injected mercury volume, mL, and V_{co} is the compressibility, which can be calculated by the helium density and slope of the linear relationship between high pressure and injected mercury volume. The coal matrix porosity can be calculated as follows:

$$\phi_{mp} = V_{mp}/(V_f + V_m + V_{mp}) \tag{16}$$

5.2. The Equipment and Process of Testing. The pore-fracture structure of the original and modified samples was measured by mercury porosimetry. The experiments were performed using a PoreMaster 33G instrument (Quantachrome, US), which permits mercury filling at as low as 0.0056, up to 204 MPa. The dried sample is evacuated to 50 mmHg or below. The volume of mercury penetration into the lump coal is measured in real time with increasing pressure. To determine the pore size distribution, a surface tension of 485 dyn/cm with a contact angle of 130° was used in the Washburn equation, eq 17.

$$r = \frac{-2\delta \cos\theta}{P} \tag{17}$$

where P is the mercury pressure, MPa, and r is the pore diameter corresponding to pressure P, μm. All this work is in the absence of confining stress.

In addition, the surface structure of the polished cube samples in the anodic, intermediate, and cathodic zones both before and after treatment was measured by SEM analysis. The experiments for SEM analysis were performed using a TM-1000 Instrument (Hitachi, Japan).

AUTHOR INFORMATION

Corresponding Author

Junqing Guo − *Key Laboratory of in Situ Property-Improving Mining of Ministry of Education, Taiyuan University of Technology, Taiyuan 030024, People's Republic of China;* orcid.org/0000-0003-1357-5906; Email: tyutzhangxiaoyu@outlook.com

Authors

Xiaoyu Zhang − *Research Institute of Mine Big Data, China Coal Research Institute, Beijing 100013, People's Republic of China; State Key Laboratory of Coal Mining and Clean Utilization, Beijing 100013, People's Republic of China*

Chunsheng Lu − *School of Civil and Mechanical Engineering, Curtin University, Western Australia 6845, Australia;* orcid.org/0000-0002-7368-8104

Zhaoyun Chai − *Key Laboratory of in Situ Property-Improving Mining of Ministry of Education, Taiyuan University of Technology, Taiyuan 030024, People's Republic of China*

Guanxian Kang − *College of Safety and Emergency Management Engineering, Taiyuan University of Technology, Taiyuan 030024, People's Republic of China*

Guofei Zhao − *Key Laboratory of in Situ Property-Improving Mining of Ministry of Education, Taiyuan University of Technology, Taiyuan 030024, People's Republic of China*

Tianhe Kang − *Key Laboratory of in Situ Property-Improving Mining of Ministry of Education, Taiyuan University of Technology, Taiyuan 030024, People's Republic of China;* orcid.org/0000-0003-2391-1969

Shirui Zhang − *Shanxi Guoyuan Coalbed Methane Comprehensive Utilization Engineering Technology Co., LTD, Taiyuan 030032, People's Republic of China*

Hengzhong Li − *Shanxi Guoyuan Coalbed Methane Comprehensive Utilization Engineering Technology Co., LTD, Taiyuan 030032, People's Republic of China*

Complete contact information is available at: https://pubs.acs.org/10.1021/acsomega.1c07286

Notes

The authors declare no competing financial interest.

ACKNOWLEDGMENTS

This research was supported financially by the National Natural Science Foundation of China (Grant Nos. 51674173, U1810102, 42072203, 51974193), Basic Research Project of Shanxi Province (Grant No. 20210302123148), and Shanxi General Youth Fund Project (Grant No. 201901D211452).

REFERENCES

(1) Li, Y.; Yang, J.; Pan, Z.; Meng, S.; Wang, K.; Niu, X. Unconventional natural gas accumulations in stacked deposits:a discussion of upper paleozoic coal-bearing strata in the east margin of the Ordos Basin, China. *Acta Geologica Sinica* **2019**, *93* (1), 111−129.

(2) Lu, Y.; Liu, Y.; Li, X.; Kang, Y. A new method of drilling long boreholes in low permeability coal by improving its permeability. *Int. J. Coal Geol.* **2010**, *84*, 94−102.

(3) Close, J.; Law, B. E.; Rice, D.D.1 Natural fractures in coal. *AAPG Stu. Geol.* **1993**, *38*, 119−132.

(4) Yuan, L. Theory of pressure-relieved gas extraction and technique system of integrated coal production and gas extraction. *J. China Coal Soc.* **2009**, *34*, 1−8.

(5) Zhang, J. Numerical simulation of hydraulic fracturing coalbed methane reservoir. *Fuel* **2014**, *136*, 57−61.

(6) Wang, T.; Zhou, W.; Chen, J.; Xiao, X.; Li, Y.; Zhao, X. Simulation of hydraulic fracturing using particle flow method and application in a coal mine. *Int. J. Coal Geol.* **2014**, *121*, 1−13.

(7) Zhao, Y.; Yang, D.; Hu, Y.; Duan, K.; Feng, Z.; Zhao, L. Study on the effective technology way for mining methane in low permeability coal seam. *J. China Coal Soc.* **2001**, *26*, 455−458.

(8) Yan, F.; Lin, B.; Zhu, C.; Shen, C.; Zou, Q.; Guo, C.; Liu, T. A novel ECBM extraction technology based on the integration of

hydraulic slotting and hydraulic fracturing. *J. Natural Gas Sci. Eng.* **2015**, *22*, 571−579.
(9) Zhang, L.; Kang, T.; Kang, J.; Zhang, X.; Zhang, B.; Chai, Z.; Zhang, R.; Wang, Y.; Kang, G.; Zhao, G. Effect of Cyclical Microwave Modification on the Apparent Permeability of Anthracite: A Case Study of Methane Extraction in Sihe Mine, China. *ACS omega* **2021**, *6*, 15001−15011.
(10) Kumar, H.; Lester, E.; Kingman, S.; Bourne, R.; Avila, C.; Jones, A.; Robinson, J.; Halleck, P.; Mathews, J. Inducing fractures and increasing cleat apertures in a bituminous coal under isotropic stress via application of microwave energy. *Int. J. Coal Geol.* **2011**, *88*, 75−82.
(11) Guo, D.; Pei, H.; Song, J.; Qin, F.; Liu, X. Study on splitting mechanism of coal bed deep hole cumulative blasting to improve permeability. *J. China Coal Soc.* **2008**, *33*, 1381−1385.
(12) Li, Z.; Wang, D.; Song, D. Influences of temperature on dynamic diffusion coefficient of CH_4 into coal particles by new diffusion model. *J. China Coal Soc.* **2015**, *40*, 1055−1064.
(13) Zou, Y.; Zhang, S.; Zhang, J. Damage mechanism of coal powder on fracture conductivity. *J. China Coal Soc.* **2012**, *37*, 1890−1894.
(14) Bodden, W. R.; Ehrlich, R. Permeability of coal and characteristics of desorption tests: implications for coalbed methane production. *Int. J. Coal Geol.* **1998**, *35*, 333−347.
(15) Masszi, D. Cavity stress-relief method for recovering methane from coal seams. *Rocky Mt. Assoc. Geologists* **1991**, 149−154.
(16) Eddy, G. E.; Rightmire, C. T.; Bryer, C. W. Relationship between methane content of coal rank and depth: theoretical vs. observed. *Unconventional Gas Recovery Symposium*; SPE: Pittsburgh, PA, 1982.
(17) Kang, T. *A Method of Enhancing Gas Desorption and Seepage from Coal Seam by Electrochemical Method*. CN102296982-A [P]. China, **2013**; ZL201110130935.8.
(18) Zhang, X.; Kang, T.; Hou, M.; Kang, J.; Guo, J.; Li, L.; Zhang, R.; Hu, Y. Experimental research on the effects of electrode materials on methane adsorption and desorption in anthracite modified by electrochemical treatment. *Chin. J. Geophys-CH.* **2020**, *63*, 2466−2477.
(19) Guo, J.; Kang, T.; Kang, J.; Chai, Z.; Zhao, G. Accelerating methane desorption in lump anthracite modified by electrochemical treatment. *Int. J. Coal Geol.* **2014**, *131*, 392−399.
(20) Zhang, X.; Zhang, R.; Kang, T.; Hu, Y. The adsorption and desorption behavior of CH4 on Jincheng anthracite modified in Fe^{3+} and Cu^{2+} ion electrolytes. *Energy Fuels* **2020**, *34*, 1251−1258.
(21) Kang, J. Ph.D. Thesis, Taiyuan University of Technology, 2018.
(22) Li, Y.; Lu, G.; Rudolph, V. Compressibility and fractal dimension of fine coal particles in relation to pore structure characterisation using mercury porosimetry. *Part. Part Syst. Char.* **1999**, *16*, 25−31.
(23) Spitzer, Z. Mercury porosimetry and its application to the analysis of coal pore structure. *Powder Technol.* **1981**, *29*, 177−186.
(24) Walker, P. L., Jr; Verma, S. K.; Rivera-Utrilla, J.; Davis, A. Densities, porosities and surface areas of coal macerals as measured by their interaction with gases, vapours and liquids. *Fuel* **1988**, *67*, 1615−1623.
(25) Yao, Y.; Liu, D.; Tang, D.; Tang, S.; Huang, W.; Liu, Z.; Che, Y. Fractal characterization of seepage-pores of coals from China: An investigation on permeability of coals. *Comput. Geo Sci.* **2009**, *35*, 1159−1166.
(26) Gan, H.; Nandi, P.; Walker, P. L. Nature of the porosity in American coals. *Fuel* **1972**, *51*, 272−277.
(27) Rodrigues, C. F.; Lemos de Sousa, M. J. The measurement of coal porosity with different gases. *Int. J. Coal Geol.* **2002**, *48*, 245−251.
(28) Spitzer, Z. Mercury porosimetry and its application to the analysis of coal pore structure. *Powder Technol.* **1981**, *29*, 177−186.
(29) Xie, K. *Coal Structure and Its Reactivity*; Science Press: Beijing, 2002.
(30) Li, Y.; Yang, J.; Pan, Z.; Tong, W. Nanoscale pore structure and mechanical property analysis of coal: An insight combining AFM and SEM images. *Fuel* **2020**, *260*, 116352.
(31) Li, Y.; Wang, Y.; Wang, J.; Pan, Z. Variation in permeability during CO_2-CH_4 displacement in coal seams: Part 1 - Experimental insights. *Fuel* **2020**, *263*, 116666.
(32) Mandelbrot, B. B. *The Fractal Geometry of Nature*; Freeman: San Francisco, 1982.
(33) Steele, W. A. *The Interaction of Gases with Solid Surface*; Pergamon: Oxford, 1974.
(34) Angulo, R. F.; Alvarado, V.; Gonzalez, H. Fractal dimensions from mercury intrusion capillary tests. *Latin America Petroleum Engineering Conference*; SPE, 1982.
(35) Sarkar, N.; Chaudhuri, B. B. An efficient differential box-counting approach to compute fractal dimension of image. *IEEE. T. Syst. Man CY-S.* **1994**, *24*, 115−120.
(36) Su, E.; Liang, Y.; Zou, Q. Structures and fractal characteristics of pores in long-flame coal after cyclical supercritical CO2 treatment. *Fuel* **2021**, *286*, 119305.
(37) Xia, W.; Yang, J. Changes in surface properties of anthracite coal before and after inside/outside weathering processes. *Appl. Surf. Sci.* **2014**, *313*, 320−324.
(38) Fu, X.; Qin, Y.; Xue, X. Research on fractals of pore and fracture structure of coal reservoirs. *J. China U. Min. Technol.* **2001**, *20*, 225−228.
(39) Liu, C.; Sang, S.; Zhang, K.; Song, F.; Wang, H.; Fan, X. Effects of temperature and pressure on pore morphology of different rank coals: Implications for CO2 geological storage. *J. CO2 Util.* **2019**, *34*, 343−352.
(40) Li, Z.; Lin, B.; Hao, Z.; Gao, Y.; Liu, F. Fractal characteristics of porosity for porous media in coal mass. *J. Min. Saf. Eng.* **2013**, *30*, 437−442.
(41) Pfeifer, P.; Wu, Y. J.; Cole, M. W.; Krim, J. Multilayer adsorption on a fractally rough surface. *Phys. Rev. Lett.* **1989**, *62*, 1997−2000.
(42) Washburn, E. W. The dynamics of capillary flow. *Phys. Rev.* **1921**, *17*, 273−283.
(43) Avinr, D.; Farin, D.; Pfeifer, P. A discussion of some aspects of surface fractality and of its determination. *New J. Chem.* **1992**, *16*, 439−449.
(44) Toda, Y.; Toyoda, S. Application of mercury porosimetry to coal. *Fuel* **1972**, *51*, 199−201.
(45) Zwietering, P.; Krevelen, D. W. Chemical structure and properties of coal IV-Pore structure. *Fuel* **1954**, *33*, 331−333.
(46) Guo, J.; Kang, T.; Kang, J.; Zhao, G.; Huang, Z. Effect of the lump size on methane desorption from anthracite. *J. Natural Gas Sci. Eng.* **2014**, *20*, 337−346.
(47) Zhao, A.; Liao, Y.; Tang, X. Quantitative analysis of pore structure by fractal analysis. *J. China Coal Soc.* **1998**, *23*, 439−442.
(48) Gamson, P. D.; Beamish, B. B.; Johnson, D. Coal micro-structure and micropermeability and their effects on natural gas recovery. *Fuel* **1993**, *72*, 87−99.
(49) Guo, X.; Yao, Y.; Liu, D. Characteristics of coal matrix compressibility: an investigation by mercury intrusion porosimetry. *Energy Fuel* **2014**, *28*, 3673−3678.
(50) Steel, K. M.; Besida, J.; O'Donnell, T. A.; Wood, D. G. Production of ultra clean coal Part I—Dissolution behavior of mineral matter in black coal toward hydrochloric and hydrofluoric acids. *Fuel Process. Technol.* **2001**, *70*, 171−192.
(51) Pfeifer, P.; Avnir, D. Chemistry in non integer dimensions between 2 and 3, I: fractal theory of heterogenous surface. *J. Chem. Phys.* **1983**, *79*, 3558−3565.
(52) Laubach, S. E.; Marrett, R. A.; Olson, J. E.; Scott, A. R. Characteristics and origins of coal cleat: A review. *Int. J. Coal Geol.* **1998**, *35*, 175−207.
(53) Friesen, W. I.; Mikula, R. J. Fractal dimensions of coal particles. *J. Colloid Interface Sci.* **1987**, *120*, 263−271.

https://doi.org/10.1021/acsomega.1c07286
ACS Omega 2022, 7, 11148−11157